ACS NANO

www.acsnano.org

ARTICLE

# Diameter Dependence of Water Filling in Lithographically Segmented Isolated Carbon Nanotubes

Samuel Faucher, Matthias Kuehne, Volodymyr B. Koman, Natalie Northrup, Daichi Kozawa, Zhe Yuan, Sylvia Xin Li, Yuwen Zeng, Takeo Ichihara, Rahul Prasanna Misra, Narayana Aluru, Daniel Blankschtein, and Michael S. Strano*

Cite This: *ACS Nano* 2021, 15, 2778–2790

Read Online

ACCESS | Metrics & More | Article Recommendations | Supporting Information

**ABSTRACT:** **Although the structure and properties of water under conditions of extreme confinement are fundamentally important for a variety of applications, they remain poorly understood, especially for dimensions less than 2 nm. This problem is confounded by the difficulty in controlling surface roughness and dimensionality in fabricated nanochannels, contributing to a dearth of experimental platforms capable of carrying out the necessary precision measurements. In this work, we utilize an experimental platform based on the interior of lithographically segmented, isolated single-walled carbon nanotubes to study water under extreme nanoscale confinement. This platform generates multiple copies of nanotubes with identical chirality, of diameters from 0.8 to 2.5 nm and lengths spanning 6 to 160 $\mu$m, that can be studied individually in real time before and after opening, exposure to water, and subsequent water filling. We demonstrate that, under controlled conditions, the diameter-dependent blue shift of the Raman radial breathing mode (RBM) between 1 and 8 cm$^{-1}$ measures an increase in the interior mechanical modulus associated with liquid water filling, with no response from exterior water exposure. The observed RBM shift with filling demonstrates a non-monotonic trend with diameter, supporting the assignment of a minimum of 1.81 ± 0.09 cm$^{-1}$ at 0.93 ± 0.08 nm with a nearly linear increase at larger diameters. We find that a simple hard-sphere model of water in the confined nanotube interior describes key features of the diameter-dependent modulus change of the carbon nanotube and supports previous observations in the literature. Longer segments of 160 $\mu$m show partial filling from their ends, consistent with pore clogging. These devices provide an opportunity to study fluid behavior under extreme confinement with high precision and repeatability.**

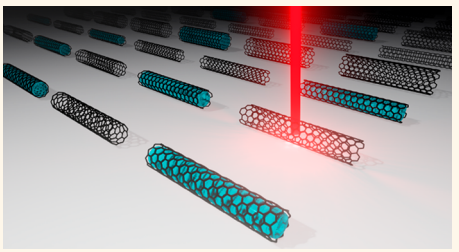

**KEYWORDS:** *carbon nanotubes, nanofluidics, nanopore, Raman spectroscopy, confinement effects, slip flow*



When confined in single-digit nanopores,[1] or pores with a characteristic dimension less than 10 nm, water displays physical properties that deviate substantially from those in larger nanopores.[2] Examples include slip flow of water inside carbon nanotubes less than 50 nm in diameter that results in flow rates that are orders of magnitude higher than those encountered in larger nanopores.[3−7] Similarly, the melting points of confined water and other fluids deviate from their values in the bulk in a diameter-dependent way described by the Gibbs−Thomson effect[8] but diverge substantially from them under extreme confinement.[9] The dielectric constant of water in graphene slit pores, too, varies widely with pore width.[10,11] Experimental observations in these exceptionally narrow nanopores have renewed interest in the study of fluids under confinement and reveal knowledge gaps in single-digit nanopore nanofluidics[1] that anticipate the development of nanofluidic devices for fundamental measurements and diverse applications. The interior of opened carbon nanotubes can serve as an experimental platform to answer these questions. However, methods do not yet exist for generating repeated and reliable comparisons of fluid filling for identical diameter single-digit nanopores of any kind. In this work, we create a platform that consists of precision nanopores in the critical diameter regime (<10 nm) formed from cut and opened ultralong carbon nanotubes (CNTs). By examining spatially dependent fluid filling repeatedly in identical systems, we can overcome impediments like pore blocking and closed

Received: October 15, 2020
Accepted: January 22, 2021
Published: January 29, 2021







https://dx.doi.org/10.1021/acsnano.0c08634
*ACS Nano* 2021, 15, 2778–2790

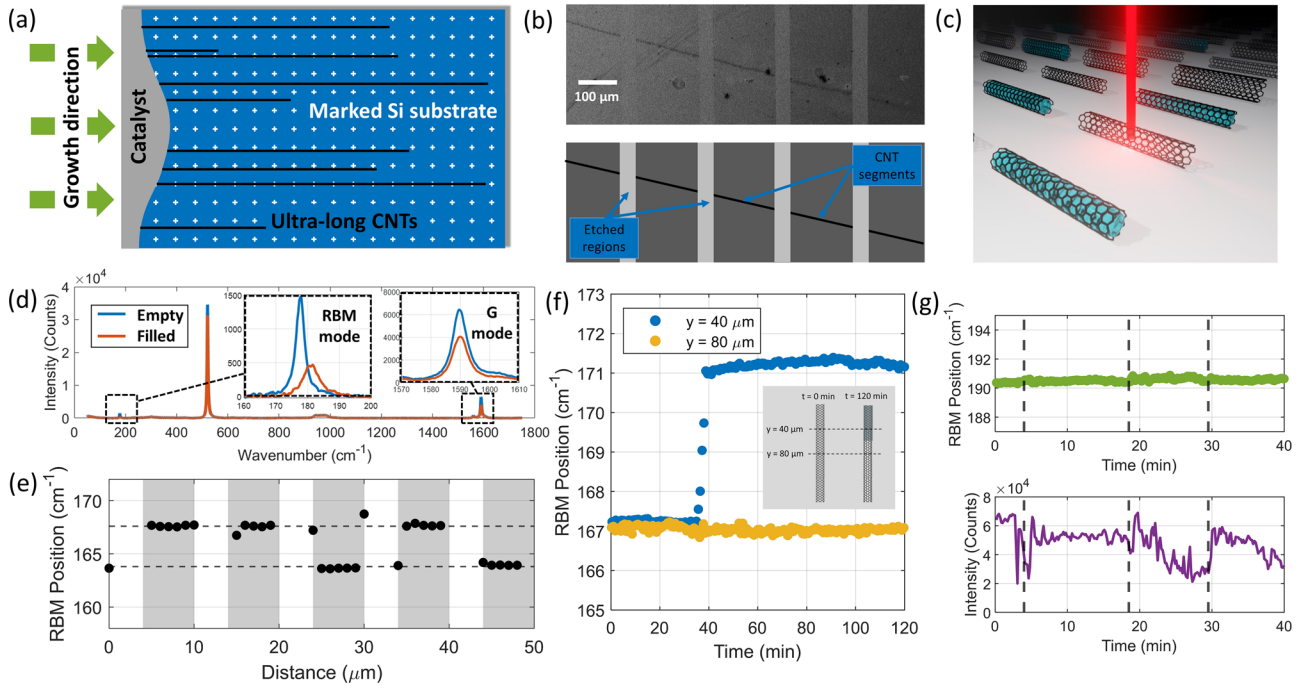


**Figure 1. Experimental platform and Raman measurements of CNT fluid filling. (a) Schematic of ultralong, vertically aligned CNTs grown by chemical vapor deposition on a marked silicon substrate. (b) Scanning electron microscopy image showing lithographic segmentation of an ultralong CNT into five independent 160 $\mu$m long, 1.38 nm diameter CNT segments of identical diameter and chirality, with accompanying schematic. (c) Illustration, not to scale, showing laser spot on empty and filled CNT segments. (d) Raman spectrum of a 1.40 nm diameter CNT in empty (blue) and filled (orange) states with RBM region and G region inset, showing upshift and broadening in RBM mode upon fluid filling. (e) Raman map of five 6 $\mu$m long, 1.52 nm diameter CNT segments produced by lithographic segmentation along their length after immersion in water. Raman spectra taken every 1 $\mu$m show two discrete vibrational states, with three filled CNT segments (with high RBM position) and two empty CNT segments (with low RBM position). (f) RBM position *versus* time at two locations ($y$ = 40 $\mu$m and $y$ = 80 $\mu$m) on a 160 $\mu$m long, 1.49 nm diameter CNT. At $t$ = 0, the sample is cooled from ambient temperature to 9 °C, causing water condensation and fluid filling at $y$ = 40 $\mu$m but not at $y$ = 80 $\mu$m, as shown by the change in Raman radial breathing mode at $y$ = 40 $\mu$m and illustrated in the accompanying schematic. (g) Exterior water does not affect the Raman radial breathing mode position, as shown by plots of RBM position and intensity *versus* time at a single location on a 1.30 nm CNT. Water droplets were added to a substrate at $t$ = 4, 18.5, and 29.5 min, causing transient increases in RBM intensity but no change in RBM position.**

CNT ends to learn fundamental aspects of confined fluid properties. This platform is relevant to carbon nanotube nanofluidics and for addressing topics including nanoscale slip flow, fluid diffusion, phase behavior, and interfacial transport that span nanofluidic device geometries and fluid types.

The fabrication of precision nanopores in the range of extreme confinement has proven difficult, limiting the number of replicates and control of pore dimensions. Two-dimensional nanochannel arrays, produced both by top-down etching of silicon and other materials and bottom-up assembly of 2D materials to form van der Waals heterostructures, comprise one class of an experimental system. Enhanced water transport in hybrid nanochannels[12] and modified interfacial behavior of water under nanoconfinement, including evaporation,[13] cavitation,[14] and vapor transport selectivity,[15] have been observed in etched Si nanochannels, though channel dimensions do not typically reach the single-digit nanometer regime. van der Waals heterostructures with graphene and other 2D materials[16,17] have addressed fundamental questions about water properties, including dielectric constant[11] and capillary condensation[18] under extreme 2D confinement, but cannot mimic the 1D confinement of nanotubes. Another class of experimental systems are multipore nanotube membranes. Carbon nanotubes membranes have been studied for close to two decades,[6,19−21] with permeation measurements showing significant flow enhancement and high slip length for membranes containing ensembles of pores with diameters in the single-digit range. CNT porins, which contain short carbon nanotubes embedded in a lipid bilayer, provide another platform for the study of water and ions through ensembles of carbon nanotubes and also show flow enhancements that vary dramatically with nanotube diameter.[5,22] This allows for precision and many replicates, but the pore length itself is extremely small (around 10 nm), causing the CNT entrance region to dominate fluid behavior. Research groups have studied water structure and phase behavior in carbon nanotube ensembles using techniques like X-ray diffraction,[23,24] allowing the proposal of a temperature-diameter phase diagram for the water−single-walled nanotube system, NMR,[25] and neutron scattering.[26,27] Spectroscopies, including IR spectroscopy,[28,29] Raman,[30−32] and photoluminescence,[31] have been used to distinguish ensembles of empty and water-filled CNTs, confirming, in some cases, the separation of the two by centrifugation.[31,33]

Only in recent years have nanofabrication techniques allowed the study of fluids in isolated, single carbon nanotubes, but to date, these experimental platforms have not allowed repeat measurements of identical CNT devices. One study by Secchi and co-workers[3] uses fluid entrainment in a Landau−Squire jet to measure flow enhancements for CNTs outside the single-digit regime from 15 to 50 nm in diameter, showing large slip lengths for CNTs and negligible slip lengths for


https://dx.doi.org/10.1021/acsnano.0c08634
ACS Nano 2021, 15, 2778−2790

boron nitride nanotubes. The difference in performance between CNTs and boron nitride nanotubes suggests that solid and interfacial properties beyond the confining diameter, like wettability and electronic structure, may affect hydrodynamics, but experimental observations of water behavior in other quasi-1D nanopores are even scarcer than those in CNTs. Additionally, the fabrication of transmembrane single carbon nanotubes does not easily extend to diameters below 10 nm, and replicates are difficult to realize.[34,35] Other studies use photoluminescence of individual solution-phase[36] or suspended CNTs[37,38] and, from our research group, Raman spectroscopy of substrate-bound CNTs[9] to observe water inside single carbon nanotube pores. Yet none of these platforms provides multiple copies of identical, localizable nanopores for repeated measurement of nanofluidic filling. The limited number of replicates or the averaging together of multiple nanopores suggest that random atomic defects, variations in pore mouth chemistry, and strongly nonmonotonic effects with confining diameter can obscure fundamental fluid properties.

Herein, we demonstrate a nanofluidic platform consisting of lithographically segmented, isolated, substrate-bound CNTs to study water under nanometer confinement. We show unequivocally that external water application and internal water filling of CNTs on silicon wafers can be distinguished by Raman spectroscopy: internal water filling causes a blue shift in the Raman radial breathing mode (RBM), whereas under these conditions, external water application does not, as shown by measurements of large numbers of isolated CNTs using air and water-immersion objectives. This creates a contrast between substrate-bound CNTs and other CNT systems—with nanotubes in solution[39,40] and suspended in vapor over a susbtrate[41]—for which the RBM mode may still change with exterior adsorption. We conclude that water filling of isolated CNTs on Si substrates is a rare, often permanent event, occurring no more than 20% of the time, and that the radial breathing mode shift upon fluid filling, $\Delta\omega_{RBM}$, varies nonmonotonically with diameter. Specifically, this RBM shift decreases to a minimum of $1.81 \pm 0.09$ cm$^{-1}$ at a diameter of $0.93 \pm 0.08$ nm before increasing for larger diameter CNTs. Although complex effects arising from the structure of water inside CNTs can be most accurately described using all-atomistic molecular simulations, here, we combine a simple hard-sphere water packing model[33,42] with an elastic shell model of the carbon nanotube[39,40] to describe the variation of $\Delta\omega_{RBM}$ with the CNT diameter. In this way, we capture the quasi-1D molecular packing effects in a simple, analytical model which can also be extended to other fluids.

## RESULTS AND DISCUSSION

The platform developed and utilized in this work is shown in Figure 1. Ultralong gas-flow aligned carbon nanotubes are grown on $SiO_2$ using a chemical vapor deposition (CVD) method developed by Huang *et al.*[43,44] as described previously by our group.[9,45] Carbon nanotubes are generally grown using a Nano-C 25 series APT carbon nanotube suspension as a catalyst solution with methane in hydrogen at 970 °C for 45 min, yielding sparse carbon nanotubes with an average pitch around 200 $\mu$m and lengths from 5 to 10 mm. A schematic showing ultralong CNTs on a marked silicon substrate is shown in Figure 1a. Samples are then etched by photolithography to produce multiple CNT segments of the same diameter and chirality. In this work, we produce and compare long (160 $\mu$m) and short (6 $\mu$m) segments. After being spin-coated with a Shipley 1805 photoresist and exposed to 60 mW/mm$^2$ at 405 nm (Heidelberg MLA150), samples are etched by low-power (6.8 W) oxygen plasma for 3 min, a technique that has been used previously for CNT etching.[46−48] A scanning electron microscopy image of several 160 $\mu$m CNT segments and an accompanying schematic are shown in Figure 1b. Other samples are instead masked with polydimethylsiloxane then etched identically by low-power oxygen plasma to produce one 2 mm long CNT segment.

In general, water filling is indicated by a shift to higher frequency of the Raman radial breathing mode of a carbon nanotube,[9,30,31,49,50] which occurs as the vibrational mode of the nanotube couples to the higher elastic modulus fluid phase. An illustration showing filled and empty CNT segments is shown in Figure 1c. A phase transition of the confined water to a phase with still higher elastic modulus—from a liquid-like to a solid-like phase, for instance—leads to further hardening of the RBM mode.[9] Figure 1d shows Raman spectra of one location on one 1.40 nm diameter CNT before and after water immersion, with RBM and G regions identified.[51] Upon interior fluid filling, the RBM peak upshifts and broadens, whereas the peak from the silicon substrate at 521 cm$^{-1}$ and the G band remain unchanged. A Raman map of five 6 $\mu$m segments of a 1.51 nm CNT is shown in Figure 1e. We can assign three segments as filled, with a high RBM position around 168 cm$^{-1}$, and two segments as empty, with a low RBM position around 164 cm$^{-1}$. Figure 1f,g shows the difference in vibrational response of a substrate-bound CNT to interior fluid filling and exterior water adsorption, respectively. Figure 1f shows interior fluid filling as tracked dynamically at two locations on a 1.49 nm carbon nanotube. In Figure 1f, the RBM position at two locations ($y$ = 40 $\mu$m and $y$ = 80 $\mu$m) on a 160 $\mu$m long, 1.49 nm diameter CNT is plotted *versus* time. At $t$ = 0, the sample is cooled to 9 °C from ambient temperature. This causes water condensation on the sample and water filling of the CNT. We see that as the fluid enters the nanotube and passes 40 $\mu$m from the end, a dynamic RBM shift occurs at time $t$ = 36 min. At 80 $\mu$m from the end, the filling profile does not reach the laser spot during the 2 h experiment, so the RBM mode does not shift. The fluid front does not reach this location likely as a result of CNT blocking or clogging. We anticipate that an experimental platform like this one, which allows tracking of fluid filling events with micron- and second-scale resolution inside isolated carbon nanotubes, could be used to analyze the dynamics of fluid filling, either as the progression of a unitary filling front with Lucas−Washburn kinetics[52,53] or the growth of fluid droplets by capillary condensation.[18,54] Figure 1g shows that exterior water, by contrast, does not cause a shift of the RBM mode. In this experiment, a single location on a 1.30 nm CNT was observed by Raman spectroscopy over time. Water droplets were added to the substrate at three times, as indicated, causing exterior CNT wetting that increases the Raman scattering cross section and the RBM intensity, as shown, but does not affect the RBM position. A sample Raman spectrum, showing background subtraction and peak fitting, is shown in supplemental Figure S1. Taken in combination, these results show the use of lithographically segmented, isolated carbon nanotubes to track interior fluid filling of CNTs spectroscopically in multiple nanofluidic devices of identical diameter.

Lithographic segmentation of ultralong CNTs allows the production of multiple copies—some empty and others


https://dx.doi.org/10.1021/acsnano.0c08634
ACS Nano 2021, 15, 2778−2790

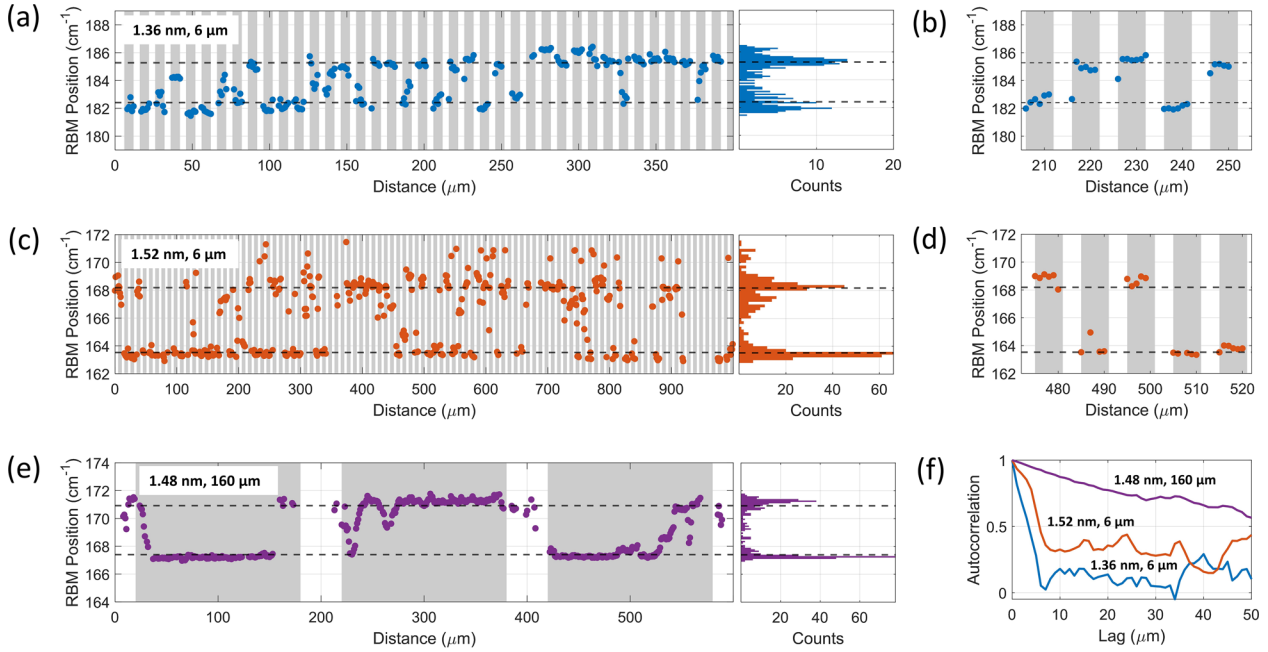


**Figure 2. Water filling in 6 $\mu$m long and 160 $\mu$m long segmented CNTs. (a) RBM position *versus* distance in 1 $\mu$m increments along 40 6 $\mu$m segments of a 1.36 nm diameter CNT at 10 $\mu$m pitch. The RBM position distribution is bimodal, with empty and filled states, as shown by the histogram at right. (b) Inset showing RBM mode over five segments of a 1.36 nm CNT. The first and fourth segments are empty, whereas the second, third, and fifth segments are water-filled. (c) RBM position *versus* distance along 100 6 $\mu$m segments of a 1.52 nm diameter CNT at 10 $\mu$m pitch. The RBM position distribution is bimodal, with empty and filled states, as shown by the histogram on the right. (d) Inset showing RBM mode over five segments of a 1.52 nm CNT. The second, fourth, and fifth segments are empty, whereas the first and third segments are water-filled. (e) RBM position *versus* distance along three 160 $\mu$m segments of a 1.48 nm diameter CNT. The first and third segments are largely empty, whereas the second segment is largely filled. The RBM position distribution is bimodal with empty and filled states, as shown by the histogram at right. (f) Autocorrelation of RBM position with lag in micrometers. The low autocorrelation in 6 $\mu$m segments at lags greater than 6 $\mu$m confirms that CNT segments fill independently. RBM position in 160 $\mu$m segments, by contrast, shows higher autocorrelation for longer lags.**

filled—of CNTs of the same diameter, chirality, and length. Fluid filling results in segmented, 6 $\mu$m long and 160 $\mu$m long CNTs are shown in Figure 2. Figure 2a shows the RBM position *versus* distance along 6 $\mu$m segments of a 1.36 nm diameter CNT. Forty segments are shown at 10 $\mu$m pitch, for a total distance of 400 $\mu$m. A histogram of RBM position is shown on the right, and an inset, showing 50 $\mu$m of distance along the nanotube axis, is shown in Figure 2b. The RBM position is distributed bimodally, with the low frequency corresponding to an empty state and the high frequency corresponding to a filled state; it is possible to assign individual segments as either filled or empty from their Raman spectra. In Figure 2b, the first and fourth segments from the left are empty, whereas the second, third, and fifth segments are filled with water. Gray and white indicate the regions that were masked from etching and exposed, respectively. The etched regions have low to nonexistent RBM and G modes, confirming successful etching. Figure 2c shows the Raman radial breathing mode frequency for 100 6 $\mu$m segments of a 1.52 nm diameter CNT, again showing empty and filled segments, with a histogram and an inset in Figure 2d. Qualitatively different filling behavior is observed for longer, 160 $\mu$m segments in Figure 2e. The RBM position is shown along three 160 $\mu$m segments of a 1.48 nm diameter CNT. The RBM states of short CNT segments are terraced as a result of entire segments being empty or filled, but longer CNT segments appear to fill from the ends but clog at some point along their length. This results in RBM modes that change within the segment. In Figure 2e, four CNT ends appear filled, one CNT end appears empty, and the filling state of one CNT end (the left of the second segment) is uncertain. The RBM position distribution is bimodal, but there are tails and shoulders in the distributions shown in Figure 2a,c,e. Specifically, in Figure 2a,c, there are three features of note in the RBM distribution: variability within 1 $cm^{-1}$ of the empty and filled peaks, weight between the two peaks, and a shoulder at a wavenumber higher than that of the filled peak. All of this RBM variation falls well within the benchmark of $\pm$2.5 $cm^{-1}$ established previously for isolated, substrate-bound CNTs.[55] Variability within 1 $cm^{-1}$ of the empty and filled peaks is commensurate with the instrument spectral resolution (0.32 $cm^{-1}$) and can be explained partly by measurement uncertainty. The rest of the spread can be explained by inhomogeneous CNT−substrate interactions, adsorbed contaminants, and other filling states. The Raman radial breathing mode is affected by interactions with a $SiO_2$ substrate, as shown by Raman comparisons of suspended and substrate-bound CNTs.[56−58] Surface roughness in the $SiO_2$ substrate, then, could cause spatial heterogeneity in CNT−$SiO_2$ van der Waals interactions that could result in smearing of the RBM peaks. An inhomogeneous distribution of adsorbed residue from the photolithography process[59,60] could also lead to smearing of the bimodal RBM position distribution. Finally, the spread in RBM could be explained by the existence of partly filled liquid-like states that fall between the empty and filled states or solid-like states that fall above the filled liquid-like state.[9] Figure 2f shows autocorrelation in RBM position *versus* lag for the three Raman maps from Figure 2a,c,e. For 6


https://dx.doi.org/10.1021/acsnano.0c08634
ACS Nano 2021, 15, 2778−2790

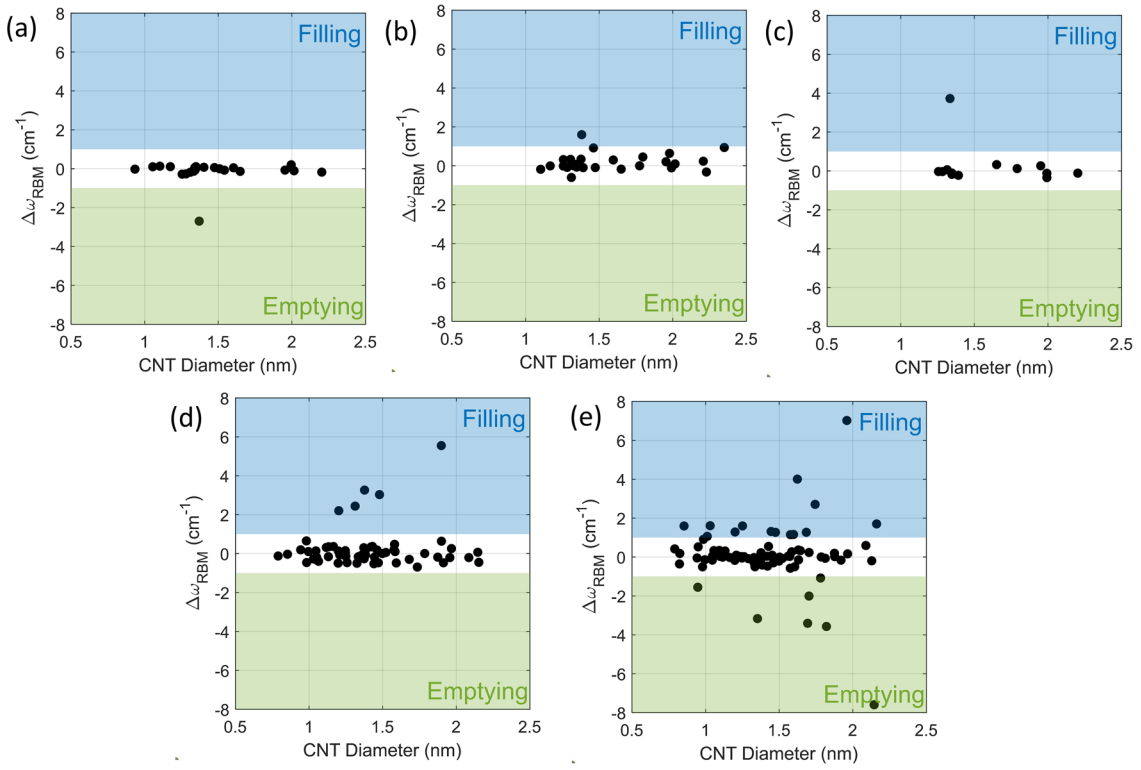


**Figure 3. Statistics of water filling of isolated carbon nanotubes. In general, each data point represents paired observations of the same location on the same chirality, 2 mm long substrate-bound CNT. (a) Change in RBM frequency *versus* CNT diameter upon remounting the sample and locating the CNT with no intervening treatment. (b) Change in RBM frequency *versus* diameter before and after 1 h $H_2O$ immersion of unetched CNT. (c) Change in RBM frequency *versus* diameter under air objective *versus* water immersion objective. (d) Change in RBM frequency *versus* diameter before and after oxygen plasma etching of CNT ends. (e) Change in RBM frequency *versus* CNT diameter before and after 1 h $H_2O$ immersion of plasma-etched CNT.**

$\mu$m segments, there is strong autocorrelation of RBM frequency for lags less than 6 $\mu$m and weak autocorrelation for lags beyond 6 $\mu$m. This suggests, as can be seen in Figure 2b,d, that RBM position is strongly correlated within each segment and largely uncorrelated between segments. The strong correlation within each segment is necessary to assign each segment as empty or filled, whereas the lack of strong correlation between segments is required to produce largely independent nanofluidic devices. Sections with several consecutive unfilled or filled CNT segments could be a result of incomplete oxygen plasma etching. By contrast, there is strong autocorrelation of the RBM position in 160 $\mu$m segments to a lag of 30−40 $\mu$m; if a location along a long CNT segment is filled or empty, that filling state may not persist along the entire segment length, but it is likely to persist for several dozen micrometers. Generation of CNT segments with lengths between 6 and 160 $\mu$m, or with lengths exceeding 160 $\mu$m, may allow more detailed study of the fraction of pore blocking events as a function of length.

In order to collect the Raman maps shown in Figure 2, we have devised an automatic setup equipped with a sub-micrometer precision mechanical stage that allows tracking of maximum Raman intensity signals, following a trace of CNTs that extend generally but not perfectly in the direction of gas flow (Figure S2). Raman *xy* maps in Figure S2a show locations of maximum intensity before and after water immersion and confirm that the location of the carbon nanotube on the substrate is the same before and after treatment. Raman maps of eight other CNT chiralities, each with 49−80 segments, generates the statistical data shown in Figure S2b. The fraction of segments that fill varies widely between samples. This could indicate some systematic blockage to fluid filling along the entire carbon nanotube: for instance, an adsorbed layer that was not fully removed during etching or an inner wall that was not resonant with the 532 nm laser and therefore was not observed. In general, these results show that chemical vapor deposition, lithography, etching, and Raman spectroscopy can be used to develop and characterize a nanofluidic platform consisting of multiple copies of the same chirality CNT of predetermined length, with some segments empty and others filled with fluid.

To clarify a point of confusion that has emerged in the literature, successive measurements taken at the same location on the same CNTs show unequivocally that observed RBM shifts are caused by interior fluid filling and not exterior water adsorption or other processes.[38] The assignment of particular spectroscopic shifts and features to CNT filling events remains controversial in some cases because Raman and photoluminescence spectroscopy are indirect probes of nano-confined water. Chiashi and co-workers suggest, for instance,[38] that the RBM shift in Agrawal *et al.*[9] is due to phase transitions of water outside the CNT rather than confined within. To address this issue, we systematically explored the effects of various conditions and treatments in the carbon nanotube filling process on the RBM mode. Figure 3 shows statistical measurements of carbon nanotube filling, where each dot represents two paired measurements made at the same location on the same diameter carbon nanotube before and after a given treatment. We define $\Delta\omega_{RBM}$ as the shift in RBM frequency in response to a certain treatment as compared to the initial state.


https://dx.doi.org/10.1021/acsnano.0c08634
*ACS Nano* 2021, 15, 2778−2790

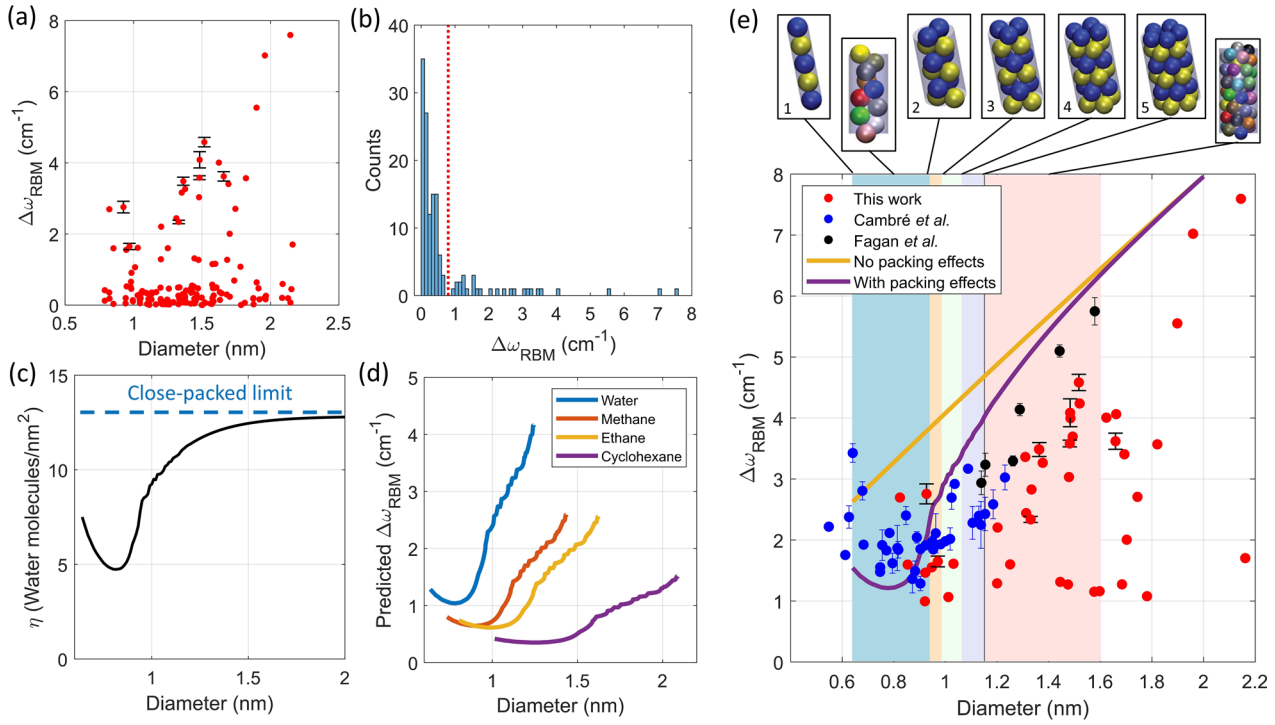


**Figure 4.** (a) Each data point represents paired observations of the same location on the same chirality, substrate-bound CNT. The absolute value of RBM shift *versus* diameter for all carbon nanotubes before and after water immersion and before and after etching is shown. Individual paired observations do not have confidence intervals, whereas repeated measurements on the same chirality CNT are shown with 95% confidence intervals. (b) Histogram showing frequency of observation of absolute shifts in RBM; $\Delta\omega_{RBM}$ = 0.8 cm$^{-1}$ (in red) was set as the threshold for water filling. (c) Areal density of water molecules per CNT surface area as a function of diameter in a hard-sphere water packing model. Water molecules are modeled as spheres with a radius of 0.15 nm in a cylinder with an excluded carbon−water radius of 0.17 nm. (d) Predicted RBM shift *versus* diameter for several fluids with an elastic shell model adapted from Longhurst and Quirke[40] with the addition of hard-sphere molecular packing effects. (e) RBM shift is shown *versus* diameter in CNTs that are presumed to have filled or emptied, with comparison to solution-phase work by Cambré *et al.*[30] and Fagan *et al.*[31] A hard-sphere water-packing model (in purple) generally captures the minimum in RBM shift at a diameter of 0.93 nm, whereas a continuum elastic shell model (in yellow) does not. The critical diameter with minimum $\Delta\omega_{RBM}$ corresponds to a minimally efficient molecular packing: a quasi-1D zigzag chain of water, as shown in schematics at top.[42] Schematics are reprinted in part with permission from ref 42. Copyright 2012 American Physical Society.

Figure 3a shows repeated Raman measurements made after the sample was removed and reloaded with no intervening treatment; the lack of shifts confirms that the CNTs do not move on the substrate, the RBM mode is stable over time, and the RBM can be measured accurately. Figure 3b shows the change in radial breathing mode frequency, $\Delta\omega_{RBM}$, before and after 1 h immersion of nonetched CNTs in water, confirming that adsorption of water to the outside of the CNT does not cause a shift in the RBM mode. This is further verified in Figure 3c, in which the RBM mode is compared with no treatment to that under a water immersion objective. Since a large majority of samples show no change, we conclude that introduction of water to the outside of a closed CNT does not affect the RBM mode for isolated CNTs on a Si wafer. Whereas other carbon nanotubes, especially those in solution and suspended, exhibit vibrational changes with exterior water adsorption,[30,38,41,61] the lack of RBM change shown here suggests that substrate-bound CNTs may already be water-saturated at ambient temperature (23 °C) and humidity (30−50%).[41,61,62] It could also suggest that interactions with the substrate or with adsorbed hydrocarbons saturate any effect that exterior water would otherwise have.

We then measured the overall filling success rate and recorded statistics associated with interior filling after a plasma etch of the CNT ends. Figure 3d shows $\Delta\omega_{RBM}$ *versus* diameter before and after oxygen plasma etching.[46−48] Although a few CNTs show the characteristic RBM upshift that we attribute to fluid filling, the number is low. It is likely that the few "filled" CNTs which filled after etching, even without water immersion, filled either (1) from ambient moisture in the air, despite environmental controls in sample processing, or (2) with acetone or isopropyl alcohol from rinsing during photoresist removal. Figure 3e, by contrast, shows a substantial number of CNTs (16/81, or 19.8%) with high $\Delta\omega_{RBM}$ before and after 1 h water immersion of pre-etched samples. For all plots, limits of $\Delta\omega_{RBM}$ = 0.8 cm$^{-1}$ for filling and −0.8 cm$^{-1}$ for emptying are proposed from the distribution of RBM shifts across all samples and by comparison to Raman results for CNT $D_2O$ filling in solution.[30] The few CNTs with a negative RBM shift upon water immersion could have been water-filled with ambient moisture and then emptied at the observed location before the second measurement, though the exact mechanism of emptying remains unclear. Since etched CNT ends and water immersion are both necessary to generate a positive RBM shift in a substantial fraction of CNTs, this shows conclusively that RBM shifts are a result of endohedral water filling and not water adsorption or other events. We observe that water filling tends to be irreversible at relevant time scales; the spectra shown were generally acquired hours after the sample was removed from water, but remain in their filled state indefinitely (*i.e.*, months) after water immersion when stored under ambient conditions. Additionally, heating


https://dx.doi.org/10.1021/acsnano.0c08634
ACS Nano 2021, 15, 2778−2790

of several samples under two conditions (150 °C, 25 mTorr, 1 h; 200 °C, $1\times10^{-4}$ Torr, 12 h) does not cause emptying, as shown by the RBM position before and after treatment.

Across the diameter range studied, CNT filling is a rare event, with most opened nanotubes not filling upon immersion in water. The fraction of CNTs that fill with water does not vary appreciably with diameter, as shown in Figure S3a. Although the success rate of CNT filling can be increased by a supplemental nitric acid treatment,[63,64] which is known to open CNT ends, as shown in Figure S3b,[65] this comes at the expense of the likely introduction of oxidative sidewall defects and altered water transport.[66] Whereas it is expected that all chiralities can, in principle, fill with water,[30] we attribute the low success rate to pore clogging: with diameters on the nanometer scale, molecular-scale impurities or unfavorable functional groups at the pore mouth can block fluid entrance, and defects and kinks in the pore body can prevent fluid from progressing through the CNT. Other experimental work shows a success rate for substrate-bound CNT opening by oxygen plasma of roughly one in three,[67] whereas solution-phase experiments eliminate the large fraction of CNTs with closed end-caps only after ultrasonication.[30] Throughout the carbon nanotube literature, use of plasma etching to open CNT ends is ubiquitous.[46,47,69−71] In many studies, without statistical sampling, it is assumed that the application of oxidative treatments results in open nanotubes with 100% certainty, but the results of our current study show otherwise. This illustrates the importance of having independent experimental confirmation that a nanopore is open and fluid-filled for nanofluidic transport applications. The platform introduced in this work, for example, allows both positive and negative controls to be studied and allows statistical analysis. It also allows the dynamics of filling to be observed, where filled and unfilled regions are identified within the same carbon nanotube.

As an application of the lithographically segmented, isolated CNT platform, we used Raman data of dozens of fluid-filled CNTs to explore the relationship between RBM shift upon fluid filling and CNT diameter. We find that this relationship is non-monotonic and suggests molecular packing effects of water inside the nanotube. The as-collected statistics of CNT water filling allows us to plot the absolute value of RBM shift *versus* CNT diameter (Figure 4a) for all CNTs before and after water immersion and before and after etching. These two treatment conditions were combined as they are the two that allow internal water filling, as discussed in Figure 3, with a large majority of filling events occurring after water immersion of etched samples. Individual paired observations are plotted without confidence intervals, whereas repeated measurements at dozens to hundreds of empty and filled locations on the same chirality CNT allow calculation of 95% confidence intervals, as shown. A histogram showing the frequency of observed RBM shifts (Figure 4b) has two peaks and a minimum between, which justifies a demarcation between empty CNTs ($|\Delta\omega_{RBM}| < 0.8$ cm$^{-1}$) and filled CNTs ($|\Delta\omega_{RBM}| > 0.8$ cm$^{-1}$). CNTs that are presumed to fill are plotted together in Figure 4e with solution-phase data from Cambré *et al.*[30] and Fagan *et al.*[31] Data from Cambré et al.,[30] in combination with data presented here and from Fagan *et al.*,[31] show that the RBM shift upon water filling passes through a minimum within the observed diameter range. Specifically, at a critical diameter of 0.93 ± 0.08 nm, a moving average of $\Delta\omega_{RBM}$ reaches a minimum of 1.81 ± 0.09 cm$^{-1}$, and its standard deviation is also minimized. Above this diameter, $\Delta\omega_{RBM}$ increases with diameter, as noted by Fagan *et al.*[31] This increase is roughly linear and extends from diameters of 1.0 to 2.2 nm for substrate-bound CNTs. Whereas most of the presented data follow the Cambré−Fagan line, certain CNTs with diameters between 1.4 and 2.2 nm fall noticeably below this line. This population of CNTs could be partly filled or could be multiwalled CNTs that fill fully but shift less due to wall−wall interactions; in either case, this population exists in substrate-bound CNT systems but not in solution. In general, it is likely imprudent to make one-to-one correspondences between observations in solution and those on a substrate in Figure 4e. This is partly due to the difficulty of assigning chiralities in substrate-supported CNTs without the benefit of a fluorescence signature and partly due to changes in the chemical environment in the two experimental systems which may lead to different observed $\Delta\omega_{RBM}$, even as the trends in $\Delta\omega_{RBM}$ with diameter appear broadly similar. Differences between the two systems highlight the need to collect more data for fluid filling of substrate-bound CNTs, particularly below 1 nm in diameter. In order to explain the observed relationship between $\Delta\omega_{RBM}$ and CNT diameter more fully, we developed a model that combines a continuum elastic shell[39,40] with discrete water size effects as inferred from spherical packing of water molecules inside a cylinder.[33,42]

As discussed by Longhurst and Quirke,[40] the RBM mode of a carbon nanotube can be modeled as a spatially uniform deformation w(t) of an elastic shell as shown below:[72]

$$\frac{w(t)}{R^2} + \frac{\rho h}{Eh}(1-\nu^2)\frac{\partial^2 w(t)}{\partial t^2} = 0 \tag{1}$$

where $t$ is time, $R$ is radius, $\rho$ is mass density, $h$ is shell thickness, $E$ is the Young's modulus, and $\nu$ is Poisson's ratio. This second-order differential equation has a solution with the following frequency:

$$\omega_0 = \frac{1}{2\pi}\left[\frac{1}{R^2}\left(\frac{Eh}{\rho h(1-\nu^2)}\right)\right]^{1/2} \tag{2}$$

Using values of $Eh = 360$ J/m$^2$, $\rho = 2.27$ g/cm$^3$, and $\nu = 0.16$ for the CNT, it is possible to recover a value of $\omega_0 = 232$ [cm$^{-1}$]/$D$ [nm] for the unperturbed radial breathing mode in this simple analytical model,[40] which is close to experimental values of $\omega_0 = 248$ [cm$^{-1}$]/$D$ [nm].[51] By extension, an elastic shell that is coupled to a second rigid elastic shell experiences spatial deformation $w(t)$ that is subject to[40]

$$\left(\frac{1}{R^2} + \frac{c}{Eh}(1-\nu^2)\right)w(t) + \frac{\rho h}{Eh}(1-\nu^2)\frac{\partial^2 w(t)}{\partial t^2} = 0 \tag{3}$$

This yields the following frequency:

$$\omega_1 = \frac{1}{2\pi}\left[\frac{1}{R^2}\left(\frac{Eh}{\rho h(1-\nu^2)}\right) + \frac{c}{\rho h}\right]^{1/2} \tag{4}$$

where $c$ is the area-normalized spring constant exerted by the rigid elastic shell on the elastic shell in question. The RBM shift upon fluid filling is the difference between the two frequencies:

$$\Delta\omega_{RBM} = \omega_1 - \omega_0 \tag{5}$$



https://dx.doi.org/10.1021/acsnano.0c08634
ACS Nano 2021, 15, 2778−2790

The interaction between the fluid and the carbon shell is captured entirely by the parameter $c$, a spring constant per unit area of CNT. We posit that the CNT−fluid interaction can be modeled as a set of independent Hookean springs between fluid molecules and a cylindrical CNT, such that the area-normalized spring constant is the product of a molecule-normalized spring constant $k$ and a fluid areal density $\eta$, expressed as

$$c = k \times \eta \tag{6}$$

where the dependencies of $k$ and $\eta$ with CNT diameter yield the $\Delta\omega_{RBM}$ *versus* $D$ relationship for a fluid−CNT pair. A schematic of this model is shown in supplemental Figure S2.

In order to determine the packing density of water in a carbon nanotube, we adapt a spherical water packing model that Cambré and Wenseleers developed to interpret density differences in fluid-filled and empty carbon nanotubes upon ultracentrifugation.[33] We estimate water as a sphere with a van der Waals radius of 0.15 nm and specify an excluded carbon−water radius of 0.17 nm.[33] Simulations of dense packing of equally sized spheres in cylinders[42,73] show that the densest arrangement of spheres in a cylinder depends on the ratio of the size of the two objects $(D/d)$ and can be uniquely determined for all states in which all spheres make contact with the confining cylinder. Within this range, there are 29 different arrangements, ranging from a single-file line at $D/d = 1$ to zigzag arrangements and more complicated arrangements as $D/d$ approaches 2.72.[42] Beyond this threshold, not all spheres make contact with the confining cylinder; this makes enumeration of sphere configurations and exact determination of geometric properties more difficult.[42] By knowing these packing arrangements, it is possible to determine a volume fraction for spherical water in a cylindrical CNT as a function of CNT diameter[33] as well as the areal molecular density $\eta$ of interior water molecules that abut the CNT wall. The areal density $\eta$, as shown in Figure 3c, has a minimum at a diameter of 0.81 nm as a result of inefficient packing of spherical water in a quasi-single-file zigzag. At very small diameters, single-file chains pack highly efficiently, whereas at large diameter, packing becomes more efficient as the cross section can accommodate more water molecules. The close-packing limit reflects the densest, hexagonal packing of circles in 2D; as the diameter of the CNT gets far larger than the diameter of the water molecules, favorable CNT−water van der Waals interactions should lead to near maximal packing of water at the almost flat CNT interface. At diameters beyond 1.2 nm, the number of possible configurations proliferates and the exact water packing arrangement is unknown, but it is possible to estimate $\eta$ from an exponential fit of the known $\eta$ toward the close-packed limit. Since water may not exactly reach this 2D packing density at high diameter, the calculated $\eta$ is an upper limit and results in a calculated upper limit for $\Delta\omega_{RBM}$ upon fluid filling.

In principle, the molecular spring constant $k$ between each water molecule and the CNT wall may also change with CNT diameter. Here, we assume that the water molecules interact with the carbon atoms of the CNT primarily through Lennard-Jones interactions, which makes it possible to obtain an analytical solution. The classic Lennard-Jones potential describes the interaction between two uncharged molecules as containing a $1/r^6$ long-range attractive term due to van der Waals forces and a $1/r^{12}$ short-range repulsive term due to orbital overlap:

$$V_{LJ} = 4\varepsilon\left[\left(\frac{\sigma}{r}\right)^{12} - \left(\frac{\sigma}{r}\right)^{6}\right] = -\frac{A}{r^6} + \frac{B}{r^{12}} \tag{7}$$

where $\varepsilon$ is the potential well depth, $\sigma$ is the characteristic Lennard-Jones distance, and $A$ and $B$ are attractive and repulsive constants. This potential can be integrated to produce a potential for the interaction of a molecule with a sheet or cylinder.[74,75] In the case of a molecule at a distance $h$ from a graphene sheet with smeared areal number density $\eta_g$ instead of discrete carbon atoms, the total potential can be written as[74]

$$E = \eta\int_S V(r)\mathrm{d}S = \eta_g\pi\left(-\frac{A}{2h^4} + \frac{B}{5h^{10}}\right) \tag{8}$$

Similarly, the potential of a particle at a distance h from the central axis of a cylinder with diameter $D$ can be expressed as[75]

$$E = \frac{3\pi D\eta_g}{16}\left(-AJ_2 + \frac{21B}{32}J_5\right) \tag{9}$$

where

$$J_n = \int_{-\pi}^{\pi}\frac{\mathrm{d}\theta}{\left(\frac{D^2}{4} + h^2 - Dh\cos\theta\right)^{n+1/2}} \tag{10}$$

The effective spring constant for a molecular interaction with a sheet or cylinder is the second derivative of the potential with distance, taken at the point of minimum potential:

$$k(r) = -\left.\frac{\partial F}{\partial r}\right|_{r=r_{eq}} = -\left.\frac{\partial^2 E}{\partial r^2}\right|_{r=r_{eq}} \tag{11}$$

Although this spring constant $k$ may vary with CNT diameter, we assume for this simple, analytical model that the variation is small, effectively using the graphene Lennard-Jones spring constant for carbon nanotubes of varying diameter. This assumption is supported by MD simulations of water inside CNTs, which show sharp density peaks at fixed distance from the CNT wall.[68] The spring constant can be calculated using water−CNT Lennard-Jones parameters[40] of $\varepsilon$ = 0.392 kJ/mol and $\sigma$ = 0.319 nm using either eq 8 or, as indicated by Cox and co-workers,[75] eq 10. The diameter at which RBM shift maxima or minima occur is sensitive to $\sigma$, which is well-established, whereas the magnitude of the predicted RBM shift is sensitive to $\varepsilon$, estimates which vary more widely in molecular dynamics simulations.[40,76]

The area-normalized spring constant $c$ can be calculated from the product of $\eta$ and $k$, allowing calculation of $\Delta\omega_{RBM}$ *versus* diameter, as shown in Figure 4e. If water packing effects are not taken into account, then $\Delta\omega_{RBM}$ increases linearly with diameter, as suggested in previous analyses.[40] If water packing effects are taken into account, then the analytical model shows a minimum in $\Delta\omega_{RBM}$ at a diameter of 0.78 nm. The experimental data, similarly, show a minimum in $\Delta\omega_{RBM}$ at a critical diameter of around 0.93 ± 0.08 nm with marked increases in $\Delta\omega_{RBM}$ on both sides of this critical diameter. The moving average and standard deviation of the experimental data is shown in gray in Figure S5. Within this range, there are five special packings of single-file (0.64 nm), double-file (0.94 nm), triple-file (0.99 nm), quadruple-file (1.06), and quintuple-file (1.15 nm) spherical water within the model CNT, as shown by the colored panels in Figure 4e.[42] These


https://dx.doi.org/10.1021/acsnano.0c08634
ACS Nano 2021, 15, 2778−2790

simple regimes are corroborated, to first order, by radial density profiles taken from molecular dynamics simulations,[68] which suggest that a diameter of 0.9 nm is the boundary between a single-file chain of water and an annular shell configuration. The region between the single-file and double-file packings (0.64 and 0.94 nm) is a zigzag, quasi-1D water structure with low volumetric fill fraction and low areal density, as shown on top in Figure 4e. As proposed by Cambré and Wenseleers,[33] the minimum in $\Delta\omega_{RBM}$ at a CNT diameter of 0.93 ± 0.08 nm is likely due to minimally efficient zigzag packing of water into the nanotube at this diameter.

This analytical treatment can be extended to the filling of CNTs with other fluids, as shown for methane, ethane, and cyclohexane in Figure 4d. This analysis neglects molecular shape, which varies among different solvents. It also assumes that the interactions between fluid molecules and a carbon nanotube can be adequately expressed as a Lennard-Jones potential, ignoring electrostatic and polarization effects[76] that may alter fluid structure and differ between strongly polar solvents like water and nonpolar solvents like methane, ethane, and cyclohexane. All-atomistic molecular dynamics simulations of CNT fluid filling, which have predominantly focused on water filling[68,76−80] with scant attention to nonaqueous fluids,[81−83] may be able to resolve interaction potentials and confined fluid densities in a way that more accurately predicts the Raman response to fluid filling. In general, this simple analytical model suggests that the Raman radial breathing mode shift upon water filling may exceed that upon filling with methane, ethane, or cyclohexane, with minima in $\Delta\omega_{RBM}$ at different diameters. Experimentally, the relative magnitude of RBM shifts upon aqueous and nonaqueous fluid filling have been reported to date for only a handful of CNT chiralities.[49]

## CONCLUSIONS

In this study, we introduced a nanofluidic platform consisting of lithographically segmented, isolated CNTs on a silicon substrate. By photolithographic segmentation, multiple copies of the same diameter and length of carbon nanotube can be subjected to the same fluidic filling conditions and monitored by Raman spectroscopy. In general, water filling events are rare and largely permanent, occurring in less than a quarter of samples. Short, 6 $\mu$m CNT segments are either filled or empty in their entirety, whereas longer 160 $\mu$m segments fill from the ends but in some cases clog along their length. We demonstrate that the Raman radial breathing mode changes only when an opened CNT is immersed in water, thus confirming that, for substrate-bound CNTs, the RBM is a sensitive measure of internal fluid filling and not of external water adsorption or other physical processes.

As an application, we used our introduced segmented CNT platform to investigate the diameter dependence of the fluid-induced upshift of the Raman radial breathing mode, $\Delta\omega_{RBM}$. Through development of an analytical shell/spring model, we were able to explain changes in the RBM shift with CNT diameter and, in particular, the minimum $\Delta\omega_{RBM}$ at a diameter of 0.93 ± 0.08 nm, as a result of changes in water packing originating from discrete size effects. As water structure changes from an efficient single-file chain to an inefficient zigzag configuration with increasing CNT diameter, $\Delta\omega_{RBM}$ decreases to a minimum of 1.81 ± 0.09 cm$^{-1}$. Then, as the diameter continues to increase, the addition of more water layers and more bulk-like water behavior causes $\Delta\omega_{RBM}$ to increase roughly linearly. These experimental results confirm the usefulness of Raman spectroscopy for tracking water filling processes in carbon nanotubes and suggest an experimental platform for the study of nonaqueous fluid filling and capillary filling dynamics under conditions of extreme quasi-1D confinement.

## METHODS

**Growth of Ultralong Aligned Carbon Nanotubes.** Ultralong gas-flow-aligned carbon nanotubes were grown by chemical vapor deposition[43] on lithographically patterned silicon substrates as described previously, with slight modifications.[9,45] To summarize, one of several catalyst solutions—iron chloride (Sigma-Aldrich) or 25 series APT carbon nanotubes (Nano-C)—was deposited on one end of a Si wafer. The sample was placed in a quartz tube, and CNTs were grown by methane CVD in hydrogen at 970 °C for 45 min.

**Lithographic Segmentation of Carbon Nanotubes.** After initial Raman scans to locate regions of interest, carbon nanotubes were segmented by photolithography. Substrates were spin-coated with a Shipley 1805 photoresist (3000 rpm); the sample was exposed (Heidelberg MLA 150 maskless aligner, 405 nm, 60 mW/mm$^2$), and the photoresist was developed (Microposit CD-26, 60 s). The sample was then etched by a low-power oxygen plasma (Harrick PDC-32G, 6.8 W) for 3 min, rinsed quickly in acetone and isopropyl alcohol to remove the photoresist, and dried at 200 °C for 5 min.

**Water and Nitric Acid Treatments.** For water treatment, samples were immersed in water (Sigma-Aldrich, ASTM Type II) for 1 h and then dried with nitrogen gas. For dynamic filling experiments, ∼10 $\mu$L of water was placed by pipet on the substrate and replenished as needed to replace losses by evaporation. For nitric acid treatment, samples were immersed in 2.6 M $HNO_3$ (Sigma-Aldrich) for 1 h before being rinsed in water and then dried at 200 °C for 5 min. Samples were stored in a desiccator chamber between experiments, with Raman spectroscopy and other measurements performed at ambient temperature (23 °C) and humidity (30−50% relative humidity).

**Characterization by Raman Spectroscopy.** As-synthesized and segmented carbon nanotubes were probed by confocal micro-Raman spectroscopy (Horiba LabRAM HR Evolution, grating 1800 gr/mm, hole 500 $\mu$m, slit 150 $\mu$m) with three different objectives (Olympus MPLFLN 50X air-immersion objective, NA = 0.8, Olympus MPLFLN 100× air-immersion objective, NA = 0.9, and Olympus LUMPLFLN 60× water-immersion objective, NA = 1.0) with a 532 nm laser (Invictus, 100 mW output power) as described previously.[9] The Raman spectrometer was arranged in a back-scattering geometry, with polarization of the incident laser parallel to the nanotube axis. Typical settings include a wavenumber range of 50 to 1750 cm$^{-1}$ and two accumulations of 5 s, with data collection using Horiba LabSpec 6 software and analyzed in Matlab. The laser spot size was 1−2 $\mu$m, depending on the objective, making it far larger than the diameter of the CNTs considered in this study, and the spectral resolution was 0.32 cm$^{-1}$. The sample was mounted on a motorized stage (Märzhäuser Wetzlar SCAN series) with $x$, $y$, and $z$ motorized control and was moved relative to the fixed laser beam.

**Data Analysis.** A scaled silicon background spectrum was subtracted from the collected spectra to remove silicon Raman features and instrument noise. Peak fitting was done in Matlab using a least-squares method to fit each RBM region and Si region to a single Lorentzian. Typical error associated with determining the peak center was 0.02 cm$^{-1}$, less than the error in instrument calibration. RBM peak position was normalized by the Si peak position in calculating $\Delta\omega_{RBM}$ to correct for any instrument miscalibration. Raman spectra that contained an RBM peak within 10 cm$^{-1}$ of one another and were captured within 10 $\mu$m of one another's nominal position during successive scans were assigned to the same CNT, with the exception that any pairs with substantially different G line shapes were rejected. CNT diameter was calculated as[84]

$$d\ [\mathrm{nm}] = \frac{248}{\omega_{RBM}\ [\mathrm{cm}^{-1}]}$$



https://dx.doi.org/10.1021/acsnano.0c08634
ACS Nano 2021, 15, 2778−2790

There are a variety of relationships between $\omega_{RBM}$ and diameter for substrate-bound SWCNTs.[85−87] More recent work[55] suggests a slightly different relationship but with an error in diameter of no more than 0.03 nm across the relevant range. Standard errors of the mean for the critical diameter and critical RBM shift were estimated by a bootstrapping method with 10,000 samples, as shown in Figure S6.

## ASSOCIATED CONTENT

### Supporting Information

The Supporting Information is available free of charge at https://pubs.acs.org/doi/10.1021/acsnano.0c08634.

Demonstration of Raman data analysis, sample Raman *xy* maps, the fraction of CNTs that fill with water and the effect of a nitric acid treatment, a schematic of the quasi-continuum filling model, Raman RBM shift *versus* diameter with a moving average, and error analysis for the critical diameter and Raman RBM shift (PDF)

## AUTHOR INFORMATION


### Corresponding Author

**Michael S. Strano** − *Department of Chemical Engineering, Massachusetts Institute of Technology, Cambridge, Massachusetts 02139, United States;* orcid.org/0000-0003-2944-808X; Email: strano@mit.edu

### Authors

**Samuel Faucher** − *Department of Chemical Engineering, Massachusetts Institute of Technology, Cambridge, Massachusetts 02139, United States;* orcid.org/0000-0002-2562-1079

**Matthias Kuehne** − *Department of Chemical Engineering, Massachusetts Institute of Technology, Cambridge, Massachusetts 02139, United States;* orcid.org/0000-0002-5096-7522

**Volodymyr B. Koman** − *Department of Chemical Engineering, Massachusetts Institute of Technology, Cambridge, Massachusetts 02139, United States*

**Natalie Northrup** − *Department of Chemical Engineering, Massachusetts Institute of Technology, Cambridge, Massachusetts 02139, United States*

**[§]Daichi Kozawa** − *Department of Chemical Engineering, Massachusetts Institute of Technology, Cambridge, Massachusetts 02139, United States;* orcid.org/0000-0002-0629-5589

**Zhe Yuan** − *Department of Chemical Engineering, Massachusetts Institute of Technology, Cambridge, Massachusetts 02139, United States;* orcid.org/0000-0002-7627-2980

**Sylvia Xin Li** − *Department of Chemical Engineering, Massachusetts Institute of Technology, Cambridge, Massachusetts 02139, United States;* orcid.org/0000-0003-2328-5259

**Yuwen Zeng** − *Department of Chemical Engineering, Massachusetts Institute of Technology, Cambridge, Massachusetts 02139, United States*

**Takeo Ichihara** − *Department of Chemical Engineering, Massachusetts Institute of Technology, Cambridge, Massachusetts 02139, United States*

**Rahul Prasanna Misra** − *Department of Chemical Engineering, Massachusetts Institute of Technology, Cambridge, Massachusetts 02139, United States;* orcid.org/0000-0001-5574-2384

**Narayana Aluru** − *Department of Mechanical Science and Engineering, University of Illinois at Urbana−Champaign, Urbana, Illinois 61801, United States;* orcid.org/0000-0002-9622-7837

**Daniel Blankschtein** − *Department of Chemical Engineering, Massachusetts Institute of Technology, Cambridge, Massachusetts 02139, United States;* orcid.org/0000-0002-7836-415X

Complete contact information is available at: https://pubs.acs.org/10.1021/acsnano.0c08634


### Notes

The authors declare no competing financial interest.

[§]Present Address: (D.K.) Quantum Optoelectronics Research Team, RIKEN Center for Advanced Photonics, Saitama 351-0198, Japan.

## ACKNOWLEDGMENTS

This work was supported as part of the Center for Enhanced Nanofluidic Transport (CENT), an Energy Frontier Research Center funded by the U.S. Department of Energy, Office of Science, Basic Energy Sciences under Award No. DE-SC0019112. S.F. acknowledges support by the National Science Foundation Graduate Research Fellowship under Grant No. 1122374. M.K. acknowledges support by the German Research Foundation (DFG) Research Fellowship KU 3952/1-1. This work was performed partly at the Center for Nanoscale Systems (CNS) at Harvard University, a member of the National Nanotechnology Infrastructure Network (NNIN), which is supported by the National Science Foundation under NSF Award No. ECS-0335765.

## REFERENCES

(1) Faucher, S.; Aluru, N.; Bazant, M. Z.; Blankschtein, D.; Brozena, A. H.; Cumings, J.; Pedro De Souza, J.; Elimelech, M.; Epsztein, R.; Fourkas, J. T.; Rajan, A. G.; Kulik, H. J.; Levy, A.; Majumdar, A.; Martin, C.; McEldrew, M.; Misra, R. P.; Noy, A.; Pham, T. A.; Reed, M. Critical Knowledge Gaps in Mass Transport through Single-Digit Nanopores: A Review and Perspective. *J. Phys. Chem. C* **2019**, *123* (35), 21309.

(2) Bocquet, L. Nanofluidics Coming of Age. *Nat. Mater.* **2020**, *19* (3), 254−256.

(3) Secchi, E.; Marbach, S.; Niguès, A.; Stein, D.; Siria, A.; Bocquet, L. Massive Radius-Dependent Flow Slippage in Carbon Nanotubes. *Nature* **2016**, *537* (7619), 210−213.

(4) Qin, X.; Yuan, Q.; Zhao, Y.; Xie, S.; Liu, Z. Measurement of the Rate of Water Translocation through Carbon Nanotubes. *Nano Lett.* **2011**, *11*, 2173−2177.

(5) Tunuguntla, R. H.; Henley, R. Y.; Yao, Y.-C.; Pham, T. A.; Wanunu, M.; Noy, A. Enhanced Water Permeability and Tunable Ion Selectivity in Subnanometer Carbon Nanotube Porins. *Science* **2017**, *357* (6353), 792−796.

(6) Holt, J.; Park, H. G.; Wang, Y.; Stadermann, M.; Artyukhin, A.; Grigoropoulos, C.; Noy, A.; Bakajin, O. Fast Mass Transport through Sub-2-Nanometer Carbon Nanotubes. *Science* **2006**, *312*, 1034−1037.

(7) Sam, A.; Hartkamp, R.; Kumar Kannam, S.; Babu, J. S.; Sathian, S. P.; Daivis, P. J.; Todd, B. D. Fast Transport of Water in Carbon Nanotubes: A Review of Current Accomplishments and Challenges. *Mol. Simul.* **2020**, 1.

(8) Shimizu, S.; Agrawal, K. V.; O'Mahony, M.; Drahushuk, L. W.; Manohar, N.; Myerson, A. S.; Strano, M. S. Understanding and Analyzing Freezing-Point Transitions of Confined Fluids within Nanopores. *Langmuir* **2015**, *31*, 10113−10118.

(9) Agrawal, K. V.; Shimizu, S.; Drahushuk, L. W.; Kilcoyne, D.; Strano, M. S. Observation of Extreme Phase Transition Temperatures

of Water Confined inside Isolated Carbon Nanotubes. *Nat. Nanotechnol.* **2017**, *12* (3), 267−273.
(10) Zhang, C.; Gygi, F.; Galli, G. Strongly Anisotropic Dielectric Relaxation of Water at the Nanoscale. *J. Phys. Chem. Lett.* **2013**, *4*, 2477.
(11) Fumagalli, L.; Esfandiar, A.; Fabregas, R.; Hu, S.; Ares, P.; Janardanan, A.; Yang, Q.; Radha, B.; Taniguchi, T.; Watanabe, K.; Gomila, G.; Novoselov, K. S.; Geim, A. K. Anomalously Low Dielectric Constant of Confined Water. *Science* **2018**, *360* (6395), 1339−1342.
(12) Xie, Q.; Alibakhshi, M. A.; Jiao, S.; Xu, Z.; Hempel, M.; Kong, J.; Park, H. G.; Duan, C. Fast Water Transport in Graphene Nanofluidic Channels. *Nat. Nanotechnol.* **2018**, *13* (3), 238−245.
(13) Li, Y.; Chen, H.; Xiao, S.; Alibakhshi, M. A.; Lo, C. W.; Lu, M. C.; Duan, C. Ultrafast Diameter-Dependent Water Evaporation from Nanopores. *ACS Nano* **2019**, *13* (3), 3363−3372.
(14) Duan, C.; Karnik, R.; Lu, M. C.; Majumdar, A. Evaporation-Induced Cavitation in Nanofluidic Channels. *Proc. Natl. Acad. Sci. U. S. A.* **2012**, *109* (10), 3688−3693.
(15) Rangharajan, K. K.; Mohana Sundaram, P.; Conlisk, A. T.; Prakash, S. Surface Dependent Enhancement in Water Vapor Permeation through Nanochannels. *Analyst* **2018**, *143* (18), 4256−4266.
(16) Geim, A. K.; Grigorieva, I. V. van der Waals Heterostructures. *Nature* **2013**, *499* (7459), 419−425.
(17) Radha, B.; Esfandiar, A.; Wang, F. C.; Rooney, A. P.; Gopinadhan, K.; Keerthi, A.; Mishchenko, A.; Janardanan, A.; Blake, P.; Fumagalli, L.; Lozada-Hidalgo, M.; Garaj, S.; Haigh, S. J.; Grigorieva, I. V.; Wu, H. A.; Geim, A. K. Molecular Transport through Capillaries Made with Atomic-Scale Precision. *Nature* **2016**, *538* (7624), 222−225.
(18) Yang, Q.; Sun, P. Z.; Fumagalli, L.; Stebunov, Y. V.; Haigh, S. J.; Zhou, Z. W.; Grigorieva, I. V.; Wang, F. C.; Geim, A. K. Capillary Condensation under Atomic-Scale Confinement. *Nature* **2020**, *588*, 250−256.
(19) Majumder, M.; Chopra, N.; Andrews, R.; Hinds, B. Enhanced Flow in Carbon Nanotubes. *Nature* **2005**, *438*, 44.
(20) Majumder, M.; Chopra, N.; Hinds, B. J. Mass Transport through Carbon Nanotube Membranes in Three Different Regimes: Ionic Diffusion and Gas and Liquid Flow. *ACS Nano* **2011**, *5* (5), 3867−3877.
(21) Wu, J.; Gerstandt, K.; Zhang, H.; Liu, J.; Hinds, B. J. Electrophoretically Induced Aqueous Flow through Single-Walled Carbon Nanotube Membranes. *Nat. Nanotechnol.* **2012**, *7* (2), 133−139.
(22) Yao, Y. C.; Taqieddin, A.; Alibakhshi, M. A.; Wanunu, M.; Aluru, N. R.; Noy, A. Strong Electroosmotic Coupling Dominates Ion Conductance of 1.5 Nm Diameter Carbon Nanotube Porins. *ACS Nano* **2019**, *13* (11), 12851−12859.
(23) Kyakuno, H.; Matsuda, K.; Yahiro, H.; Inami, Y.; Fukuoka, T.; Miyata, Y.; Yanagi, K.; Maniwa, Y.; Kataura, H.; Saito, T.; Yumura, M.; Iijima, S. Confined Water inside Single-Walled Carbon Nanotubes: Global Phase Diagram and Effect of Finite Length. *J. Chem. Phys.* **2011**, *134* (24), 244501.
(24) Kyakuno, H.; Fukasawa, M.; Ichimura, R.; Matsuda, K.; Nakai, Y.; Miyata, Y.; Saito, T.; Maniwa, Y. Diameter-Dependent Hydrophobicity in Carbon Nanotubes. *J. Chem. Phys.* **2016**, *145* (6), 064514.
(25) Hassan, J.; Diamantopoulos, G.; Gkoura, L.; Karagianni, M.; Alhassan, S.; Kumar, S. V.; Katsiotis, M. S.; Karagiannis, T.; Fardis, M.; Panopoulos, N.; Kim, H. J.; Beazi-Katsioti, M.; Papavassiliou, G. Ultrafast Stratified Diffusion of Water inside Carbon Nanotubes; Direct Experimental Evidence with 2D D−$T_2$ NMR Spectroscopy. *J. Phys. Chem. C* **2018**, *122*, 10600.
(26) Reiter, G. F.; Kolesnikov, A. I.; Paddison, S. J.; Platzman, P. M.; Moravsky, A. P.; Adams, M. A.; Mayers, J. Evidence for an Anomalous Quantum State of Protons in Nanoconfined Water. *Phys. Rev. B: Condens. Matter Mater. Phys.* **2012**, *85* (4), 45403.
(27) Briganti, G.; Rogati, G.; Parmentier, A.; Maccarini, M.; De Luca, F. Neutron Scattering Observation of Quasi-Free Rotations of Water Confined in Carbon Nanotubes. *Sci. Rep.* **2017**, *7*, 45021.
(28) Byl, O.; Liu, J.-C.; Wang, Y.; Yim, W.-L.; Johnson, J. K.; Yates, J. T. Unusual Hydrogen Bonding in Water-Filled Carbon Nanotubes. *J. Am. Chem. Soc.* **2006**, *128*, 12090−12097.
(29) Dalla Bernardina, S.; Paineau, E.; Brubach, J. B.; Judeinstein, P.; Rouzière, S.; Launois, P.; Roy, P. Water in Carbon Nanotubes: The Peculiar Hydrogen Bond Network Revealed by Infrared Spectroscopy. *J. Am. Chem. Soc.* **2016**, *138* (33), 10437−10443.
(30) Cambré, S.; Schoeters, B.; Luyckx, S.; Goovaerts, E.; Wenseleers, W. Experimental Observation of Single-File Water Filling of Thin Single-Wall Carbon Nanotubes down to Chiral Index (5,3). *Phys. Rev. Lett.* **2010**, *104* (20), 1−4.
(31) Fagan, J. A.; Huh, J. Y.; Simpson, J. R.; Blackburn, J. L.; Holt, J. M.; Larsen, B. A.; Walker, A. R. H. Separation of Empty and Water-Filled Single-Wall Carbon Nanotubes. *ACS Nano* **2011**, *5* (5), 3943−3953.
(32) Torres-Dias, A. C.; Cambré, S.; Wenseleers, W.; Machon, D.; San-Miguel, A. Chirality-Dependent Mechanical Response of Empty and Water-Filled Single-Wall Carbon Nanotubes at High Pressure. *Carbon* **2015**, *95*, 442−451.
(33) Cambré, S.; Wenseleers, W. Separation and Diameter-Sorting of Empty (End-Capped) and Water-Filled (Open) Carbon Nanotubes by Density Gradient Ultracentrifugation. *Angew. Chem., Int. Ed.* **2011**, *50* (12), 2764−2768.
(34) Marcotte, A.; Mouterde, T.; Niguès, A.; Siria, A.; Bocquet, L. Mechanically Activated Ionic Transport across Single-Digit Carbon Nanotubes. *Nat. Mater.* **2020**, *19* (10), 1057−1061.
(35) Min, H.; Kim, Y. T.; Moon, S. M.; Han, J. H.; Yum, K.; Lee, C. Y. High-Yield Fabrication, Activation, and Characterization of Carbon Nanotube Ion Channels by Repeated Voltage-Ramping of Membrane-Capillary Assembly. *Adv. Funct. Mater.* **2019**, *29* (27), 1900421.
(36) Cambré, S.; Santos, S. M.; Wenseleers, W.; Nugraha, A. R. T.; Saito, R.; Cognet, L.; Lounis, B. Luminescence Properties of Individual Empty and Water-Filled Single-Walled Carbon Nanotubes. *ACS Nano* **2012**, *6* (3), 2649−2655.
(37) Chiashi, S.; Hanashima, T.; Mitobe, R.; Nagatsu, K.; Yamamoto, T.; Homma, Y. Water Encapsulation Control in Individual Single-Walled Carbon Nanotubes by Laser Irradiation. *J. Phys. Chem. Lett.* **2014**, *5* (3), 408−412.
(38) Chiashi, S.; Saito, Y.; Kato, T.; Konabe, S.; Okada, S.; Yamamoto, T.; Homma, Y. Confinement Effect of Sub-Nanometer Difference on Melting Point of Ice-Nanotubes Measured by Photoluminescence Spectroscopy. *ACS Nano* **2019**, *13* (2), 1177−1182.
(39) Longhurst, M. J.; Quirke, N. The Environmental Effect on the Radial Breathing Mode of Carbon Nanotubes. II. Shell Model Approximation for Internally and Externally Adsorbed Fluids. *J. Chem. Phys.* **2006**, *125* (18), 184705.
(40) Longhurst, M. J.; Quirke, N. The Environmental Effect on the Radial Breathing Mode of Carbon Nanotubes in Water. *J. Chem. Phys.* **2006**, *124* (23), 234708.
(41) Chiashi, S.; Kono, K.; Matsumoto, D.; Shitaba, J.; Homma, N.; Beniya, A.; Yamamoto, T.; Homma, Y. Adsorption Effects on Radial Breathing Mode of Single-Walled Carbon Nanotubes. *Phys. Rev. B: Condens. Matter Mater. Phys.* **2015**, *91* (15), 155415.
(42) Mughal, A.; Chan, H. K.; Weaire, D.; Hutzler, S. Dense Packings of Spheres in Cylinders: Simulations. *Phys. Rev. E* **2012**, *85*, 51305.
(43) Huang, S.; Cai, X.; Liu, J. Growth of Millimeter-Long and Horizontally Aligned Single-Walled Carbon Nanotubes on Flat Substrates. *J. Am. Chem. Soc.* **2003**, *125* (19), 5636−5637.
(44) Huang, S.; Woodson, M.; Smalley, R.; Liu, J. Growth Mechanism of Oriented Long Single Walled Carbon Nanotubes Using "Fast-Heating" Chemical Vapor Deposition Process. *Nano Lett.* **2004**, *4* (6), 1025−1028.
(45) Choi, W.; Ulissi, Z. W.; Shimizu, S. F. E. E.; Bellisario, D. O.; Ellison, M. D.; Strano, M. S. Diameter-Dependent Ion Transport


https://dx.doi.org/10.1021/acsnano.0c08634
*ACS Nano* 2021, 15, 2778−2790

through the Interior of Isolated Single-Walled Carbon Nanotubes. *Nat. Commun.* **2013**, *4* (2397), 1−8.
(46) Lobo, A. O.; Ramos, S. C.; Antunes, E. F.; Marciano, F. R.; Trava-Airoldi, V. J.; Corat, E. J. Fast Functionalization of Vertically Aligned Multiwalled Carbon Nanotubes Using Oxygen Plasma. *Mater. Lett.* **2012**, *70*, 89−93.
(47) Huang, S.; Dai, L. Plasma Etching for Purification and Controlled Opening of Aligned Carbon Nanotubes. *J. Phys. Chem. B* **2002**, *106* (14), 3543−3545.
(48) Lee, C. Y.; Choi, W.; Han, J.-H. H.; Strano, M. S. Coherence Resonance in a Single-Walled Carbon Nanotube Ion Channel. *Science (Washington, DC, U. S.)* **2010**, *329* (5997), 1320−1324.
(49) Campo, J.; Piao, Y.; Lam, S.; Stafford, C. M.; Streit, J. K.; Simpson, J. R.; Hight Walker, A. R.; Fagan, J. A. Enhancing Single-Wall Carbon Nanotube Properties through Controlled Endohedral Filling. *Nanoscale Horizons* **2016**, *1* (4), 317−324.
(50) Wenseleers, W.; Cambré, S.; Čulin, J.; Bouwen, A.; Goovaerts, E. Effect of Water Filling on the Electronic and Vibrational Resonances of Carbon Nanotubes: Characterizing Tube Opening by Raman Spectroscopy. *Adv. Mater.* **2007**, *19* (17), 2274−2278.
(51) Dresselhaus, M.; Dresselhaus, G.; Saito, R.; Jorio, K. Raman Spectroscopy of Carbon Nanotubes. *Phys. Rep.* **2005**, *409*, 47−99.
(52) Washburn, E. W. The Dynamics of Capillary Flow. *Phys. Rev.* **1921**, *17* (3), 273−283.
(53) Dimitrov, D. I.; Milchev, A.; Binder, K. Capillary Rise in Nanopores: Molecular Dynamics Evidence for the Lucas-Washburn Equation. *Phys. Rev. Lett.* **2007**, *99* (5), 1−4.
(54) Zhong, J.; Riordon, J.; Zandavi, S. H.; Xu, Y.; Persad, A. H.; Mostowfi, F.; Sinton, D. Capillary Condensation in 8 nm Deep Channels. *J. Phys. Chem. Lett.* **2018**, *9* (3), 497−503.
(55) Zhang, D.; Yang, J.; Yang, F.; Li, R.; Li, M.; Ji, D.; Li, Y. (N, m) Assignments and Quantification for Single-Walled Carbon Nanotubes on $SiO_2$/Si Substrates by Resonant Raman Spectroscopy. *Nanoscale* **2015**, *7*, 10719.
(56) Zhang, Y.; Zhang, J.; Son, H.; Kong, J.; Liu, Z. Substrate-Induced Raman Frequency Variation for Single-Walled Carbon Nanotubes. *J. Am. Chem. Soc.* **2005**, *127* (49), 17156−17157.
(57) Zhang, Y.; Son, H.; Zhang, J.; Dresselhaus, M. S.; Kong, J.; Liu, Z. Raman Spectra Variation of Partially Suspended Individual Single-Walled Carbon Nanotubes. *J. Phys. Chem. C* **2007**, *111* (5), 1983−1987.
(58) Steiner, M.; Freitag, M.; Tsang, J. C.; Perebeinos, V.; Bol, A. A.; Failla, A. V.; Avouris, P. How Does the Substrate Affect the Raman and Excited State Spectra of a Carbon Nanotube? *Appl. Phys. A: Mater. Sci. Process.* **2009**, *96* (2), 271−282.
(59) Gotovac, S.; Honda, H.; Hattori, Y.; Takahashi, K.; Kanoh, H.; Kaneko, K. Effect of Nanoscale Curvature of Single-Walled Carbon Nanotubes on Adsorption of Polycyclic Aromatic Hydrocarbons. *Nano Lett.* **2007**, *7* (3), 583−587.
(60) Cunha, R.; Paupitz, R.; Yoon, K.; Van Duin, A. C. T.; Elías, A. L.; Carozo, V.; Dasgupta, A.; Fujisawa, K.; Lopez, N. P.; Araujo, P. T.; Terrones, M. Raman Spectroscopy Revealing Noble Gas Adsorption on Single-Walled Carbon Nanotube Bundles. *Carbon* **2018**, *127*, 312−319.
(61) Homma, Y.; Chiashi, S.; Yamamoto, T.; Kono, K.; Matsumoto, D.; Shitaba, J.; Sato, S. Photoluminescence Measurements and Molecular Dynamics Simulations of Water Adsorption on the Hydrophobic Surface of a Carbon Nanotube in Water Vapor. *Phys. Rev. Lett.* **2013**, *110* (15), 157402.
(62) Edwards, P. J.; Wang, B.; Cronin, S. B.; Bushmaker, A. W. Direct Measurement of Water-Assisted Ion Desorption and Solvation on Isolated Carbon Nanotubes. *ACS Nano* **2020**, *14* (12), 16854−16863.
(63) Zhang, J.; Zou, H.; Qing, Q.; Yang, Y.; Li, Q.; Liu, Z.; Guo, X.; Du, Z. Effect of Chemical Oxidation on the Structure of Single-Walled Carbon Nanotubes. *J. Phys. Chem. B* **2003**, *107* (16), 3712−3718.
(64) Tchoul, M. N.; Ford, W. T.; Lolli, G.; Resasco, D. E.; Arepalli, S. Effect of Mild Nitric Acid Oxidation on Dispensability, Size, and Structure of Single-Walled Carbon Nanotubes. *Chem. Mater.* **2007**, *19* (23), 5765−5772.
(65) Tsang, S. C.; Chen, Y. K.; Harris, P. J. F. F.; Green, M. L. H. H. A Simple Chemical Method of Opening and Filling Carbon Nanotubes. *Nature* **1994**, *372* (6502), 159−162.
(66) Majumder, M.; Corry, B. Anomalous Decline of Water Transport in Covalently Modified Carbon Nanotube Membranes. *Chem. Commun.* **2011**, *47*, 7683−7685.
(67) Rabinowitz, J.; Cohen, C.; Shepard, K. L. An Electrically Actuated, Carbon-Nanotube-Based Biomimetic Ion Pump. *Nano Lett.* **2020**, *20* (2), 1148.
(68) Pascal, T. A.; Goddard, W. A.; Jung, Y. Entropy and the Driving Force for the Filling of Carbon Nanotubes with Water. *Proc. Natl. Acad. Sci. U. S. A.* **2011**, *108* (29), 11794−11798.
(69) Zschoerper, N. P.; Katzenmaier, V.; Vohrer, U.; Haupt, M.; Oehr, C.; Hirth, T. Analytical Investigation of the Composition of Plasma-Induced Functional Groups on Carbon Nanotube Sheets. *Carbon* **2009**, *47* (9), 2174−2185.
(70) Mathur, A.; Roy, S. S.; Hazra, K. S.; Wadhwa, S.; Ray, S. C.; Mitra, S. K.; Misra, D. S.; McLaughlin, J. A. Oxygen Plasma Assisted End-Opening and Field Emission Enhancement in Vertically Aligned Multiwall Carbon Nanotubes. *Mater. Chem. Phys.* **2012**, *134* (1), 425−429.
(71) Pang, P.; He, J.; Park, J. H.; Krstić, P. S.; Lindsay, S. Origin of Giant Ionic Currents in Carbon Nanotube Channels. *ACS Nano* **2011**, *5* (9), 7277−7283.
(72) Wang, C. Y.; Ru, C. Q.; Mioduchowski, A. Free Vibration of Multiwall Carbon Nanotubes. *J. Appl. Phys.* **2005**, *97* (11), 114323.
(73) Pickett, G. T.; Gross, M.; Okuyama, H. Spontaneous Chirality in Simple Systems. *Phys. Rev. Lett.* **2000**, *85* (17), 3652−3655.
(74) Chan, Y.; Hill, J. M. Modelling Interaction of Atoms and Ions with Graphene. *Micro Nano Lett.* **2010**, *5* (5), 247−250.
(75) Cox, B. J.; Thamwattana, N.; Hill, J. M. Mechanics of Atoms and Fullerenes in Single-Walled Carbon Nanotubes. II. Oscillatory Behaviour. *Proc. R. Soc. London, Ser. A* **2007**, *463* (2078), 477−494.
(76) Misra, R. P.; Blankschtein, D. Insights on the Role of Many-Body Polarization Effects in the Wetting of Graphitic Surfaces by Water. *J. Phys. Chem. C* **2017**, *121*, 28166.
(77) Hummer, G.; Rasaiah, J. C.; Noworyta, J. P. Water Conduction through the Hydrophobic Channel of a Carbon Nanotube. *Nature* **2001**, *414* (6860), 188−190.
(78) Barati Farimani, A.; Aluru, N. R. Existence of Multiple Phases of Water at Nanotube Interfaces. *J. Phys. Chem. C* **2016**, *120* (41), 23763−23771.
(79) Suk, M. E.; Aluru, N. R. Modeling Water Flow through Carbon Nanotube Membranes with Entrance/Exit Effects. *Nanoscale Microscale Thermophys. Eng.* **2017**, *21* (4), 247−262.
(80) Nomura, K.; Kaneko, T.; Bai, J.; Francisco, J. S.; Yasuoka, K.; Zeng, X. C. Evidence of Low-Density and High-Density Liquid Phases and Isochore End Point for Water Confined to Carbon Nanotube. *Proc. Natl. Acad. Sci. U. S. A.* **2017**, *114* (16), 4066−4071.
(81) Supple, S.; Quirke, N. Molecular Dynamics of Transient Oil Flows in Nanopores I: Imbibition Speeds for Single Wall Carbon Nanotubes. *J. Chem. Phys.* **2004**, *121* (17), 8571−8579.
(82) Supple, S.; Quirke, N. Molecular Dynamics of Transient Oil Flows in Nanopores. II. Density Profiles and Molecular Structure for Decane in Carbon Nanotubes. *J. Chem. Phys.* **2005**, *122* (10), 104706.
(83) Kondratyuk, P.; Wang, Y.; Liu, J.; Johnson, J. K.; Yates, J. T. Inter- and Intratube Self-Diffusion in *n*-Heptane Adsorbed on Carbon Nanotubes. *J. Phys. Chem. C* **2007**, *111* (12), 4578−4584.
(84) Jorio, A.; Saito, R.; Hafner, J. H.; Lieber, C. M.; Hunter, M.; McClure, T.; Dresselhaus, G.; Dresselhaus, M. S. Structural (n, m) Determination of Isolated Single-Wall Carbon Nanotubes by Resonant Raman Scattering. *Phys. Rev. Lett.* **2001**, *86* (6), 1118−1121.
(85) Yang, F.; Wang, M.; Zhang, D.; Yang, J.; Zheng, M.; Li, Y. Chirality Pure Carbon Nanotubes: Growth, Sorting, and Characterization. *Chem. Rev.* **2020**, *120* (5), 2693−2758.


https://dx.doi.org/10.1021/acsnano.0c08634
*ACS Nano* 2021, 15, 2778−2790

(86) Jungen, A.; Popov, V. N.; Stampfer, C.; Durrer, L.; Stoll, S.; Hierold, C. Raman Intensity Mapping of Single-Walled Carbon Nanotubes. *Phys. Rev. B: Condens. Matter Mater. Phys.* **2007**, *75* (4), 041405.
(87) Araujo, P. T.; Maciel, I. O.; Pesce, P. B. C.; Pimenta, M. A.; Doorn, S. K.; Qian, H.; Hartschuh, A.; Steiner, M.; Grigorian, L.; Hata, K.; Jorio, A. Nature of the Constant Factor in the Relation between Radial Breathing Mode Frequency and Tube Diameter for Single-Wall Carbon Nanotubes. *Phys. Rev. B: Condens. Matter Mater. Phys.* **2008**, *77* (24), 2−5.



https://dx.doi.org/10.1021/acsnano.0c08634
*ACS Nano* 2021, 15, 2778−2790